The Relationship between [207]Pb NMR Chemical Shift and Solid-State Structure in Pb(II) Compounds

O. Dmitrenko,[†] Shi Bai,[†] Peter A. Beckmann,[†,‡] Scott van Bramer,[§] Alexander J. Vega,[†] and C. Dybowski[†]

Department of Chemistry and Biochemistry, University of Delaware, Newark, Delaware 19716, Department of Physics, Bryn Mawr College, Bryn Mawr, Pennsylvania 19010, and Department of Chemistry, Widener University, Chester, Pennsylvania 19013

The analysis of heavy-metal solids with NMR spectroscopy provides a means of investigating the electronic environment through the dependence of the chemical shift on structure. We have investigated the relation of the [207]Pb NMR isotropic chemical shift, span, and skew of a series of solid Pb(II) compounds to lattice parameters. Complementary relativistic spin−orbit density functional calculations on clusters such as PbI_6^{4-} that model the local environment in the dihalides show a dependence of NMR properties on the local structure in good agreement with experimental results.

I. Introduction

The [207]Pb nuclear magnetic resonance (NMR) spectroscopy of solid lead-containing materials has recently been investigated by several groups.[1−15] These results indicate some general trends: (1) The range of isotropic chemical shift extends over approximately 10 000 ppm. (2) The isotropic shift depends strongly on the local electronic structure making the lead NMR chemical shift a sensitive reporter of local state.[9] (3) The [207]Pb resonance in many ionic materials tends to be more strongly shielded than in organolead materials. (4) The range of the principal elements of the chemical shift tensor at a single site may be as large as several thousand ppm showing the striking dependence of the chemical shift on local structure.[9] (5) The chemical shift can be correlated with other structural parameters such as interatomic distance[10] or electronegativity difference between lead and its ionic partners.[5,9] (6) For certain materials such as $Pb(NO_3)_2$, the chemical shift parameters vary significantly with temperature,[12,13] which engenders the use of the lead NMR as a thermometric reporter. (7) Application of external pressure causes large changes in the shift parameters.[14]

In this paper, we report the dependence of the experimental chemical shift tensor parameters (isotropic shift, span, and skew[16,17]) of $PbMoO_4$ and $PbCl_2$ on temperature and reconsider the thermal behavior of these parameters for $Pb(NO_3)_2$. The experimental variation of the isotropic shift and the span with temperature is strongly correlated with the thermal expansion in these materials from which one may infer the dependence of NMR parameters on unit cell dimensions.

Density functional (DFT) calculations of the electronic structure of cluster models of lead-containing solids, incorporating relativistic effects with the zero-order regular approximation (ZORA), have also been performed. The calculations predict chemical shifts of the series of lead dihalides that are in reasonable agreement with experimental values. NMR simulations on a cluster model, $[PbI_6]^{4-}$, that has several different reported structural motifs show a dependence of chemical shift

parameters on the lead−iodide distance ($r_{Pb−I}$) analogous to the experimentally determined dependence of chemical shift on cell dimension observed for $PbMoO_4$, $PbCl_2$, and $Pb(NO_3)_2$.

II. Experiments and Calculations

The $PbMoO_4$ and $PbCl_2$ samples were purchased from Sigma-Aldrich and were used without further purification. The quoted purity of the materials was 99.9999%. The $Pb(NO_3)_2$ sample was the same as used elsewhere.[4,7]

[207]Pb NMR spectra were measured as a function of temperature at 62.6 MHz on a Bruker MSL-300 NMR spectrometer (7.0491 T, corresponding to a ^{1}H resonance frequency of $\omega_o/2\pi = 300.130$ MHz, with a $\pi/2$ pulse width of 2.8 μs) or at 41.7 MHz on a TecMag Discovery NMR spectrometer (4.6954 T, corresponding to a ^{1}H resonance frequency of $\omega_o/2\pi = 199.916$ MHz, with a $\pi/2$ pulse width of 4.2 μs). Phase cycling, data processing, and fitting procedures have been previously reported.[5−7,18] All NMR spectra are referred to the isotropic chemical shift of liquid $Pb(CH_3)_4$ using the chemical shift of $Pb(NO_3)_2$ at the peak of the powder pattern as a secondary reference.[6,13d]

Temperatures above room temperature were achieved by blowing heated nitrogen gas over the sample. Temperatures below room temperature were achieved by blowing heated cold nitrogen gas boiled off from a liquid-nitrogen source. Temperature was measured by monitoring the ^{1}H spectrum of a very small (0.04 mL) volume of ethylene glycol ($HO(CH_2)_2OH$) (above room temperature) or methanol (CH_3OH) (at or below room temperature).[19] For measurements at 62.6 MHz on the Bruker MSL 300, these liquids were contained in small glass bulbs that were included in the sample chamber. For measurements at 41.7 MHz on the TecMag Discovery, the variable temperature system was calibrated with these liquids in separate experiments. The Fourier transform spectra at all temperatures *T* were fitted to theoretical powder patterns with a program developed in this laboratory to obtain the chemical shift parameters as discussed previously.[18]

Cluster models based on X-ray structures in the Inorganic Crystal Structure Database (ICSD)[20] were used to perform

[†] University of Delaware.
[‡] Bryn Mawr College.
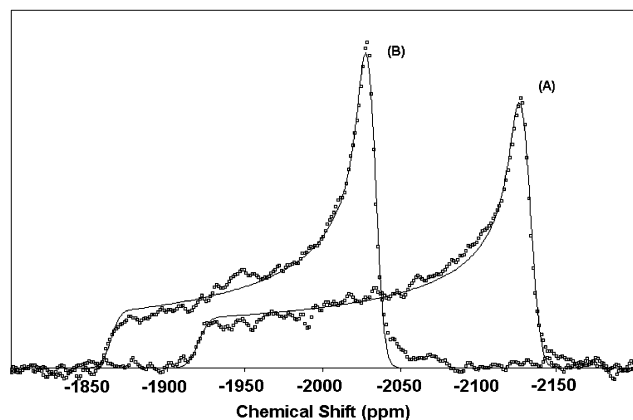[§] Widener University.

Figure 1. The solid-state NMR spectra of static polycrystalline PbMoO$_4$ at $\omega_o/2\pi = 62.6$ MHz. Solid lines indicate the fitted spectra. Both spectra were produced using a 50 kHz spectral window. Spectrum A is the sum of 24 scans with a recycle time of 85 s at $T = 188$ K, and the values of the fitted chemical shift parameters are $\delta_{iso} = -2028$ ppm and $\Omega = 209$ ppm. Spectrum B results from the coaddition of 200 scans with a recycle time of 29 s at $T = 354$ K and is fitted with $\delta_{iso} = -1988$ ppm and $\Omega = 165$ ppm.

density function (DFT) calculations of the electronic structures of several compounds. The DFT calculations, carried out with the Amsterdam Density Function program package[21] and its associated NMR module,[22,23] incorporated relativistic effects with the zero-order regular approximation (ZORA)[21-26] and triple-ζ (ZORA/TZ2P) basis sets. All atoms were treated without frozen cores. The module DIRAC was applied to generate the core potentials for all atom types. We used the local density approximation (LDA) of Vosko, Wilk, and Nusair (VWN)[24] augmented with the Becke88−Perdew86 generalized gradient approximation (GGA) (BP86) facility.[25,26] Diamagnetic, paramagnetic, and spin-orbital contributions to the chemical shielding were summed to give the total chemical shielding. The shielding of tetramethyllead Pb(CH$_3$)$_4$ [TML] was calculated within the same model, using the experimental geometry,[27] and all chemical shifts are reported relative to TML.

The NMR chemical shift is a second-rank symmetric tensor. There are several ways to express the tensor information. A common means is specification of the three principal elements of the tensor, δ_{11}, δ_{22}, and δ_{33}, with the convention that

$$\delta_{11} \geq \delta_{22} \geq \delta_{33} \qquad (1)$$

In this report, we use the IUPAC-recommended notation in which the following three quantities are defined in terms of the principal elements of the chemical shift tensor.[16,28]

$$\delta_{iso} = \frac{1}{3}(\delta_{11} + \delta_{22} + \delta_{33}) \qquad (2)$$

$$\Omega = \delta_{11} - \delta_{22} \qquad (3)$$

and

$$\kappa = \frac{3(\delta_{22} - \delta_{iso})}{\Omega} \qquad (4)$$

These three quantities are the isotropic chemical shift, the span, and the skew, respectively.

III. Results

Experimental Chemical Shifts. Figure 1 shows 62.6 MHz [207]Pb spectra of a powder sample of PbMoO$_4$ at 188 and 354 K and Figure 2 shows 41.7 MHz [207]Pb spectra of PbCl$_2$ at 297 and 365 K. A room-temperature spectrum of Pb(NO$_3$)$_2$ appears elsewhere,[6] and the temperature dependence of the spectrum has been investigated.[13d,29]

The dependence of δ_{iso} on temperature T for Pb(NO$_3$)$_2$ has been reported to give a linear dependence,[6,13d] which can be expressed as

$$\delta_{iso} = \delta_{iso,RT} + \left[\frac{d\delta_{iso}}{dT}\right](T - T_{RT}) \qquad (5)$$

where room-temperature T_{RT} is 295 K and $\delta_{iso,RT}$ is δ_{iso} at T_{RT}. The constant $\delta_{iso,RT}$ and the slope $d\delta_{iso}/dT$ are given in Table 1. The span Ω of Pb(NO$_3$)$_2$ at three temperatures has been reported by Bielecki and Burum.[29] Those data and additional measurements by us are shown in Figure 3. The data obey the equation

$$\Omega = \Omega_{RT} + \left[\frac{d\Omega}{dT}\right](T - T_{RT}) \qquad (6)$$

where the subscript RT again means room temperature (295 K). Ω_{RT} and $d\Omega/dT$ for Pb(NO$_3$)$_2$ are given in Table 1. Because of the 3-fold rotation site symmetry, κ for Pb(NO$_3$)$_2$ is fixed at +1, and this value was assumed in the data fitting.

δ_{iso} and Ω for PbMoO$_4$, shown in Figure 4, are fitted to eqs 5 and 6 to obtain the slopes and room-temperature values given in Table 1. The room-temperature values are the same as the values of Van Bramer et al.[5] By point symmetry of the lead site, κ for PbMoO$_4$ is fixed at −1, which was assumed in the data fitting.

δ_{iso} and Ω for PbCl$_2$, shown in Figure 5, are also fitted to eqs 5 and 6. The slopes and room-temperature values are given in Table 1. Because κ for PbCl$_2$ is not required by the lead site symmetry to have a specific value, the powder spectra were fit to the general asymmetric pattern allowing all three variables to change. Over the temperature range studied, $\kappa = 0.505 \pm 0.023$, independent of temperature within experimental error, as indicated in Figure 5C.

The temperature dependencies of the unit cell dimensions of Pb(NO$_3$)$_2$,[30] PbMoO$_4$,[31] and PbCl$_2$[32] have been determined by

TABLE 1: Experimental Values and Derivatives Involving the Isotropic Chemical Shift, Span, Temperature, and Characteristic Length of Pb(NO$_3$)$_2$, PbMoO$_4$, and PbCl$_2$

	unit	Pb(NO$_3$)$_2$	PbMoO$_4$	PbCl$_2$
$d\delta_{iso}/dT$	ppm/K	0.758 ± 0.002	0.494 ± 0.026	0.976 ± 0.043
$\delta_{iso,RT}$	ppm	-3490 ± 1	-2005 ± 2	-1721 ± 2
$d\Omega/dT$	ppm/K	-0.224 ± 0.004	-0.255 ± 0.019	-0.912 ± 0.087
Ω_{RT}	ppm	52.5 ± 0.3	183 ± 1	556 ± 4
dL/dT	10^{-5} nm/K	2.07 ± 0.02	1.13 ± 0.02	2.000 ± 0.005
L_{RT}	nm	0.784^a	0.708^a	0.677^a
$d\delta_{iso}/dL$	10^4 ppm/nm	3.658 ± 0.045	4.35 ± 0.32	4.89 ± 0.18
$d\Omega/dL$	10^4 ppm/nm	-1.079 ± 0.050	-2.30 ± 0.22	-4.56 ± 0.17

^{a} The uncertainties in L_{RT} are less than 1 part in 10^4.
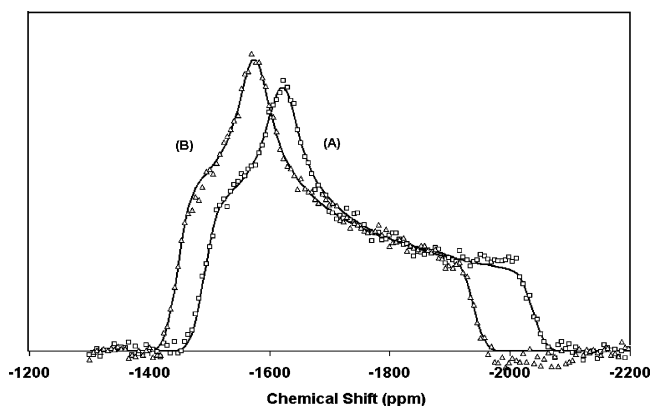
Figure 2. The solid-state NMR spectra of static polycrystalline $PbCl_2$ at $\omega_o/2\pi = 41.7$ MHz. Solid lines indicate the fitted spectra. Both spectra were produced using a 37.6 kHz spectral window, and each spectrum results from the coaddition of 512 scans with a recycle time of 15 s. Spectrum A was obtained at $T = 297$ K, and the values of the fitted chemical shift parameters are $\delta_{iso} = -1716$ ppm and $\Omega = 543$ ppm. Spectrum B was obtained at 365 K, and the values of the fitted chemical shift parameters are $\delta_{iso} = -1653$ ppm and $\Omega = 484$ ppm.
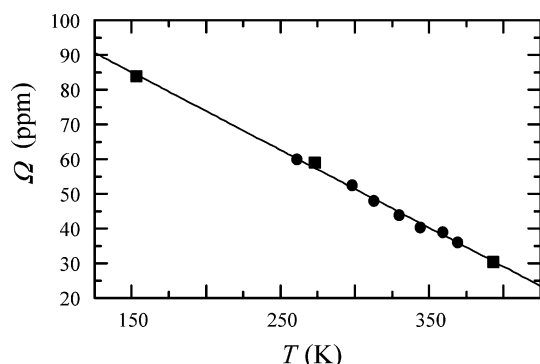

Figure 3. The temperature T dependence of the span Ω for Pb-$(NO_3)_2$: ●, 62.6 MHz (this work); ■, ref 29. The solid line is the best-fit linear relation as given in eq 6 with the parameters given in Table 1.

X-ray diffraction. It is convenient to characterize the unit cell at a temperature by a characteristic length $L = V^{1/3}$, where V is the volume of the unit cell. As an example, the temperature dependence of L for $PbMoO_4$ is plotted in Figure 6 and is fitted to

$$L = L_{RT} + \left[\frac{dL}{dT}\right](T - T_{RT}) \tag{7}$$

with the room-temperature values L_{RT} and the slopes dL/dT given in Table 1. Similar plots can be made for $Pb(NO_3)_2$ and $PbCl_2$, and the slopes and room-temperature values are given in Table 1.

The linear dependencies in eqs 5 and 6 and the linear dependence in eq 7 allow the NMR parameters δ_{iso} and Ω to be expressed in terms of L.

$$\delta_{iso} = \delta_{iso,RT} + \left[\frac{d\delta_{iso}}{dL}\right](L - L_{RT}) \tag{8}$$

and

$$\Omega = \Omega_{RT} + \left[\frac{d\Omega}{dL}\right](L - L_{RT}) \tag{9}$$

The resulting slopes $d\delta_{iso}/dL$ and $d\Omega/dL$ for the three compounds are given in Table 1.

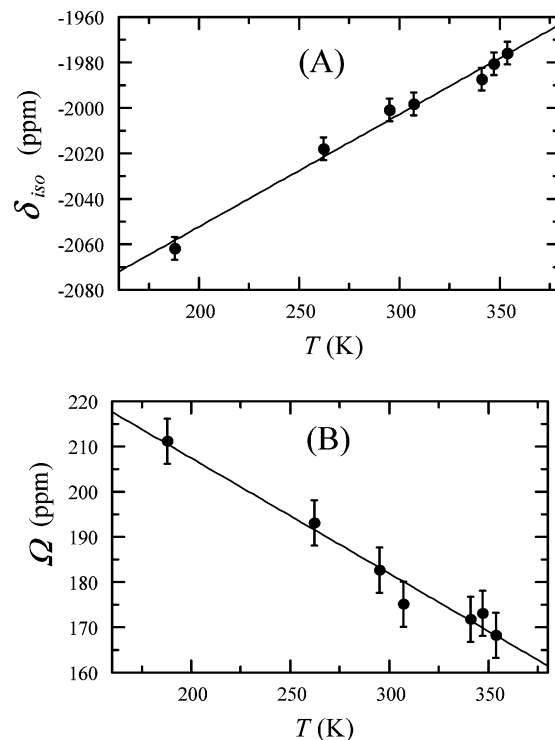**Figure 4.** The temperature T dependence of (A) the isotropic chemical shift δ_{iso} and (B) the span Ω of $PbMoO_4$ determined at 62.6 MHz. These parameters are obtained from fitting the experimentally obtained spectra as indicated in Figure 1. The solid lines are the best-fit linear relations as given by eqs 5 and 6 in the text.

Model Cluster Calculations. Relativistic DFT chemical shift calculations for molecular structures such as PbX_4 (X = Cl, Br, I) have been shown to give reasonable agreement with experimental measurements[23] as have calculations of molecular adducts of lead[15] and ^{139}La chemical shifts in lanthanum halides.[33] Solid materials such as the lead dihalides exist in extended arrays that periodically repeat. To make the calculation of the properties of these solid materials tractable, we have modeled the local structures with clusters, PbX_n^{2-n}, of the dihalides PbX_2 (X = F, Cl, Br, I) that are based on reported X-ray structures. The number of atoms included in the cluster, the ICSD number of the X-ray data,[20] and the chemical shift results are given in Table 2. The agreement of the calculated δ_{iso} with experimental isotropic shifts for the dihalide structures is good as can be seen in Figure 7.

To investigate the change in parameters as a function of structure, we have calculated the NMR parameters of PbI_6^{4-} (representing the local environment in PbI_2). PbI_2 was chosen for this purpose because it has a well-defined local structure (a distorted octahedron with a single Pb–I distance, Figure 8) with a clear distinction between nearest neighbor Pb–I distances r_{Pb-I} and next-nearest neighbor distances. In addition, a range of crystal structures of PbI_2 presents an opportunity to study the changes in chemical shift parameters under realistic structure variations. These reported structures each have a single value of r_{Pb-I} between 0.298 and 0.323 nm and a single value of θ between 0.205° and 10.88° as indicated in Table 2. The next-nearest neighbors are about 0.56 nm from the Pb nucleus. The rhombohedral distortion can be completely described by the Pb–I distance r_{Pb-I} and a bond angle deviation θ from 90°.
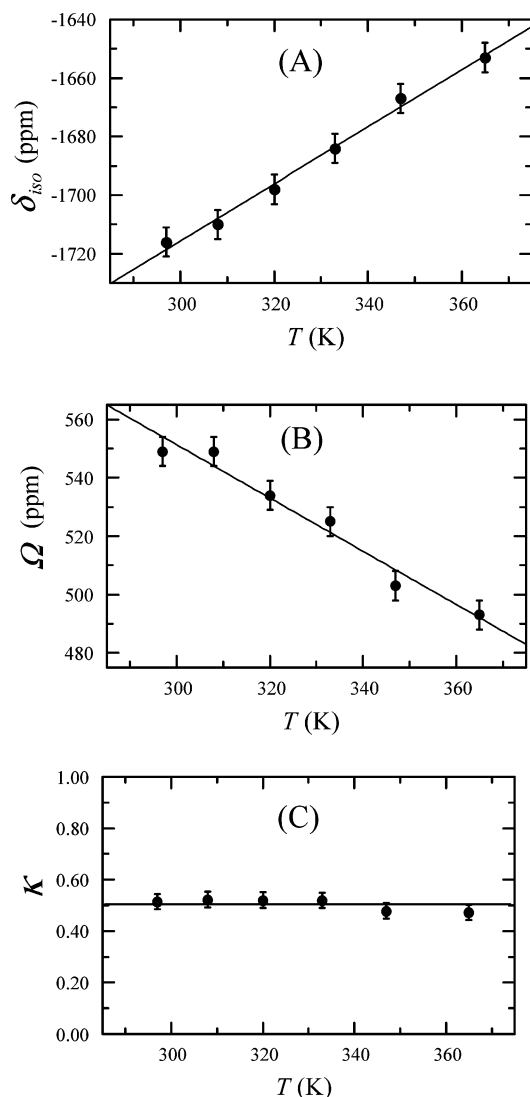
[207]Pb NMR Chemical Shift and Solid-State Structure

J. Phys. Chem. A, Vol. 112, No. 14, 2008 **3049**
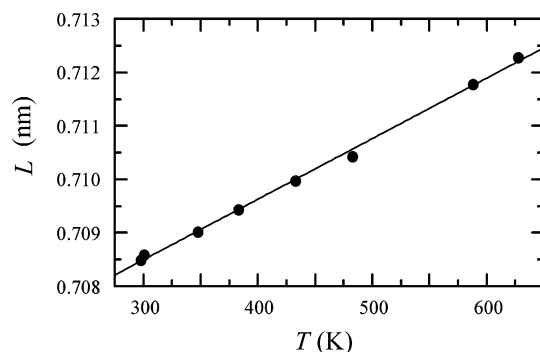

Figure 6. *L*, the cube root of the volume of the unit cell in crystalline $PbMoO_4$ as a function of temperature *T* taken from X-ray diffraction data.[31] The solid line is the best-fit linear relation as given by eq 7.
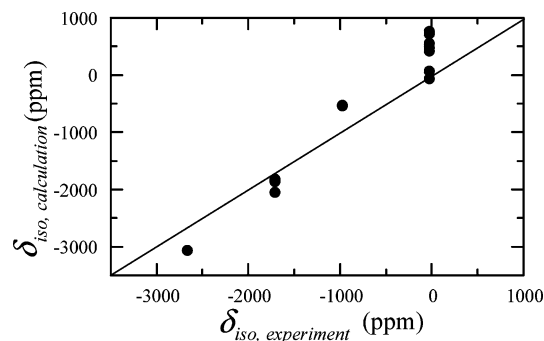

Figure 7. $\delta_{iso,calculation}$ versus $\delta_{iso,experiment}$ (both referenced to $Pb(CH_3)_4$) for PbF_2, $PbCl_2$, $PbBr_2$, and PbI_2. The values of $\delta_{iso,calculation}$ are given in Table 2. The values of $\delta_{iso,experiment}$ are taken from ref 8 for all four compounds. For comparison, the line $\delta_{iso,calculation} = \delta_{iso,experiment}$ is shown.

Figure 5. The temperature *T* dependence of the NMR parameters of $PbCl_2$: (A) the isotropic chemical shift δ_{iso}, (B) the span Ω, and (C) the skew κ determined at a frequency of 41.7 MHz. These parameters are obtained from fitting the experimental spectra as indicated in Figure 2. The solid lines for δ_{iso} and Ω are the best-fit linear relations as given by eqs 5 and 6 in the text. κ appears to be temperature independent from the results of fitting, the average value being 0.505 ± 0.023.

δ_{iso} for PbI_6^{4-} is shown as a function of r_{Pb-I} in Figure 9A. The data in Figure 9A can be fitted to the linear equation

$$\delta_{iso} = \delta_{iso,0} + \left[\frac{d\delta_{iso}}{dr_{Pb-I}}\right](r_{Pb-I} - r_{Pb-I,0}) \quad (10)$$

where $r_{Pb-I,0} = 0.310$ nm is a convenient reference distance. The slope $d\delta_{iso}/dr_{Pb-I}$ and the constant $\delta_{iso,0}$ (the isotropic shift at $r = r_{Pb-I,0}$) are given in Table 3. Ω as a function of θ, shown in Figure 9B, is also linear and is fitted to

$$\Omega = \left[\frac{d\Omega}{d\theta}\right]\theta + \Omega_o \quad (11)$$

with $d\Omega/d\theta$ and Ω_o given in Table 3. In Figure 9C, we show the dependence of Ω on r_{Pb-I}. Although, as Figure 9B shows, Ω is a linear function of θ, it is convenient to discuss its variation as a function of the interatomic distance. As discussed in the following section, we are interested in $d\Omega/dr_{Pb-I}$ in very small Δr_{Pb-I} regions (Figure 9C) from -0.4×10^4 ppm nm^{-1}

in a region centered around $r_{Pb-I} = 0.320$ nm to -1.4×10^4 ppm nm^{-1} in a region centered around $r_{Pb-I} = 0.300$ nm in Figure 9C. These limiting slopes are reported in Table 2.

IV. Discussion

The measured temperature dependencies of the isotropic shift and span of the [207]Pb chemical shift parameters of $Pb(NO_3)_2$, $PbMoO_4$, and $PbCl_2$ (Table 1) are linear functions of the characteristic length *L* in the range of temperature we investigated. The skew of the $PbCl_2$ resonance (for which symmetry does not require $\kappa = \pm 1$) is, within experimental error, independent of temperature. Of particular note is the general trend that the isotropic chemical shift increases with increasing unit cell size and that the span decreases with increasing unit cell size.

Insight into the direct effects of structural parameters on the chemical shift tensor components and its contributors (paramagnetic, diamagnetic, and spin−orbit) can be obtained from DFT-ZORA calculations on model clusters.[15,22,23] The reasonably good agreement between the calculated isotropic chemical shifts of the lead dihalides and their room-temperature experimental values (Figure 7) reinforces our confidence in the usefulness of calculations on clusters to model the local environment of a [207]Pb nucleus in these solids. The agreement between calculation and experiment strongly suggests that the geometric parameters of the Pb ion's immediate environment are the principal structural determinants of the chemical shift tensor components.[15] The results indicate that both the paramagnetic and spin−orbit contributions affect the variation of the chemical shift, but the paramagnetic contribution dominates. The diamagnetic contribution remains almost constant in all models (Table S1 in the Supporting Information).

TABLE 2: Ionic Clusters of PbX_2 (X = F, Cl, Br, and I) Used in the Calculations: ICSD Codes,[a] Model Fragments, Geometrical Characteristics, and Calculated ^{207}Pb NMR Parameters

ICSD #	model fragment	r_{Pb-I} (nm)	θ (degrees)	Ω (ppm)	δ_{iso} (ppm)
			PbI_2		
42 013	$[PbI_6]^{4-}$	0.323	0.205	2.1	780.3
23 762	$[PbI_6]^{4-}$	0.323	0.225	2.9	725.4
77 324	$[PbI_6]^{4-}$	0.318	1.231	15.6	559.3
42 510	$[PbI_6]^{4-}$	0.316	2.394	31.5	482.6
52 370	$[PbI_6]^{4-}$	0.314	2.465	32.6	433.3
77 325	$[PbI_6]^{4-}$	0.303	7.081	106.5	76.1
30 347	$[PbI_6]^{4-}$	0.298	10.88	179.8	−62.4
			$PbBr_2$		
202 134	$[PbBr_9]^{7-}$	[b]	[b]	811.8	−527.2
36 170	$[PbBr_9]^{7-}$	[b]	[b]	876.9	−531.9
			$PbCl_2$		
52 346	$[PbCl_9]^{7-}$	[b]	[b]	959.8	−1826.7
43 344	$[PbCl_9]^{7-}$	[b]	[b]	531.9	−1832.5
202 130	$[PbCl_9]^{7-}$	[b]	[b]	620.7	−1854.0
15 806	$[PbCl_9]^{7-}$	[b]	[b]	580.2	−1864.4
27 736	$[PbCl_9]^{7-}$	[b]	[b]	627.5	−1864.5
81 976	$[PbCl_9]^{7-}$	[b]	[b]	561.4	−2061.3
			PbF_2		
14324	$[PbF_9]^{7-}$	[b]	[b]	220.9	−3076.1
24 523	$[PbF_8]^{6-}$	[b]	[b]	0.0	−3076.4

[a] From ref 19. [b] In view of the complex structure of $PbBr_2$, $PbCl_2$, and PbF_2 model clusters, there are multiple distances and angles. Therefore, there are no single value data for distances, and bond angles are not meaningful.
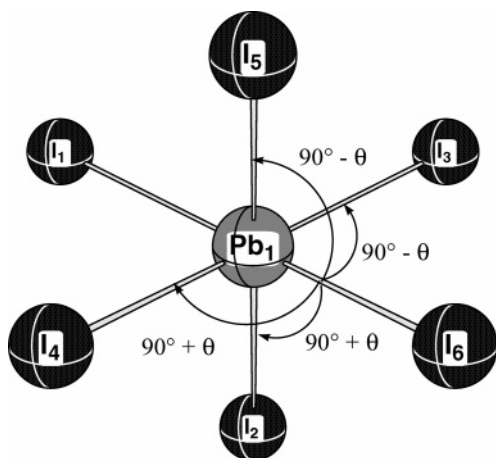

Figure 8. The PbI_6^{4-} fragment representing the local environment of a Pb nucleus in a PbI_2 crystal. The structure of the fragment is a rhombohedrally distorted octahedron possessing a single 3-fold roto-inversion axis. It has six equal Pb—I distances r_{Pb-I}, six I—Pb—I angles that are smaller than 90° by θ, and six I—Pb—I angles that are larger than 90° by the same deviation. The angle θ is a measure of deviation from octahedral symmetry. See Table 2. The body diagonal of the vectors connecting Pb with I_2, I_4, and I_6 is the 3-fold symmetry axis.

TABLE 3: Calculated Values and Derivatives of the Isotropic Chemical Shift and Span for a PbI_6^{4-} Cluster

	unit	PbI_6^{4-}
$d\delta_{iso}/dr_{Pb-I}$	10^4 ppm/nm	3.30 ± 0.12
δ_{iso} at r_{Pb-I} = 0.31 nm	ppm	318 ± 12
$d\Omega/dr_{Pb-I}$	10^4 ppm/nm	−0.4 to −1.4
$d\Omega/d\theta$	ppm/degree	4.7 ± 2.4

The DFT calculations are carried out at a fixed average structure. As such, the effects of vibrations are not considered explicitly in the results in Tables 2 and 3. The vibrational amplitude of atoms in an ionic lattice is about 0.005 nm.[34] Since the chemical shifts are found to be linear functions of the lattice dimension over comparable ranges, the average over the vibrational motion is expected to be the same as the chemical shift calculated at the average structure.

The calculated chemical shift parameters of the PbI_6^{4-} cluster are quite sensitive to the structure of the local environment as can be seen in Figure 9 by the range of isotropic chemical shifts calculated for the PbI_6^{4-} clusters that were reported by X-ray crystallography. As seen in Figure 9A, over this range, the calculated isotropic chemical shift is a linear ascending function of r_{Pb-I}, the lead—iodide distance. This is indicative of a trend of the lead resonance toward reduced shielding when interatomic distances increase. As seen in Figure 9B, the span Ω is linearly proportional to θ over the same range of structure variation, indicating that the deviation of the shift tensor from spherical symmetry depends primarily on the deviation of the cluster from octahedral symmetry, consistent with a speculation by Sharma et al. on the angular dependence of ^{205}Tl NMR parameters of $TlPbI_3$.[2] On the other hand, the relationship of Ω with the interatomic distance is not linear as seen in Figure 9C. It reflects the nonlinear relationship between θ and r_{Pb-I} of the X-ray structures and indicates that the angular distortion of the cluster has a more direct effect on the span than the interatomic distance has.

One may understand the approach of the span to zero in Figure 9C qualitatively by noting that the structure becomes more nearly octahedral as r_{Pb-I} increases. These DFT derived predictions agree with the experimental results on $Pb(NO_3)_2$, $PbMoO_4$, and $PbCl_2$ in that, as the characteristic length L increases, the isotropic shift increases and the span decreases. The experimental results do not reveal a noticeable deviation from a linear relationship between span and lattice expansion, most probably because the range of L in the measurements (∼0.003 nm) is much smaller than the range of r_{Pb-I} (∼0.03 nm) in Figure 9C.

The characteristic dimension, L, is a measure of the size of the unit cell, whereas the interatomic distance r_{Pb-I} measures a single distance in a cluster. These two measures are not directly comparable. However, r_{Pb-I} is always smaller than L by a factor of approximately 2−3. Keeping this difference in mind, one sees that the experimentally determined slopes $d\delta_{iso}/dL$ in Table 1 are within a factor of 1.1−1.5 of the calculated slope
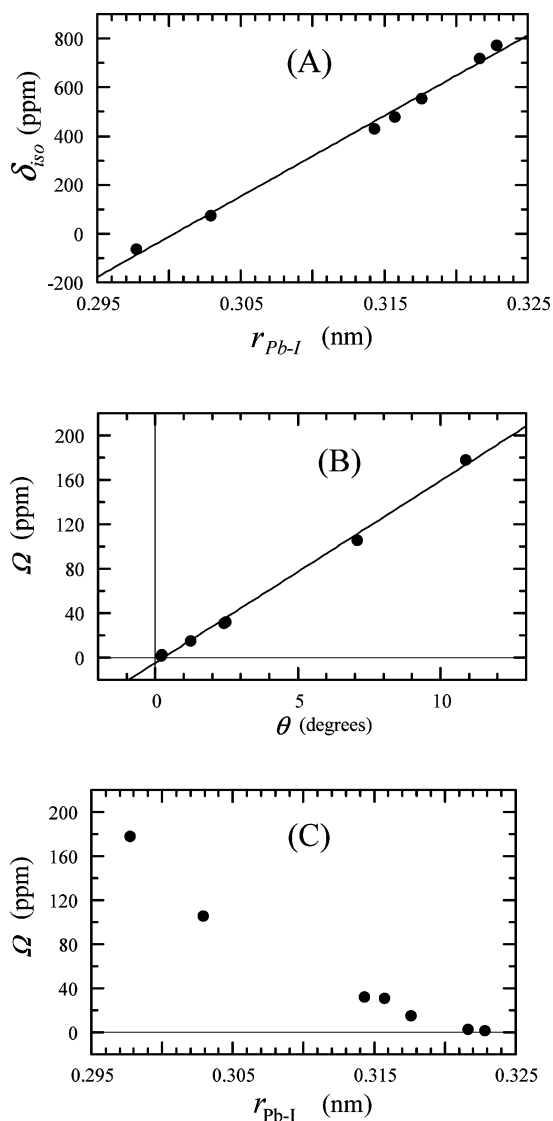
[207]Pb NMR Chemical Shift and Solid-State Structure

J. Phys. Chem. A, Vol. 112, No. 14, 2008 **3051**

Figure 9. Calculated NMR parameters of a PbI_6^{4-} cluster using ZORA-DFT techniques. (A) δ_{iso} versus r_{Pb-I}, (B) Ω versus θ, and (C) Ω versus r_{Pb-I}.

$d\delta_{iso}/dr_{Pb-I}$ in Table 3. It is significant that the calculated and experimental slopes of the isotropic chemical shift are all positive and that the span decreases with expansion of the cell.

The relation between chemical shift and lattice dimensions has also been addressed by Zwanziger et al., who recently reported experimental and ab initio results for chemical shielding in crystals under pressure.[14] Particularly relevant to our work are their theoretical results for [207]Pb shielding under hydrostatic pressure applied to the cubic structures of PbS, PbSe, and PbTe. They introduce a coefficient Z_{iso} to quantify the effect of pressure, P, on the shielding

$$\Delta\sigma_{iso} = Z_{iso}P \qquad (12)$$

The authors relate Z_{iso} to the bulk modulus B of the material.[14] The pressure dependence in eq 12 can be converted to a distance dependence by using the definition of the bulk modulus as the ratio of the pressure to the fractional volume change, $P = -B\Delta V/V$, and by replacing $\Delta V/V$ by $3\Delta L/L$, L being the characteristic dimension of the unit cell. The change in chemical shielding, $\Delta\sigma_{iso}$, is tantamount to the negative of the change in isotropic chemical shift. The results of Zwanziger et al.[14] can

therefore be expressed as the derivative of the isotropic chemical shift with respect to the characteristic dimension

$$\frac{d\delta_{iso}}{dL} = \frac{3Z_{iso}B}{L} \qquad (13)$$

For PbS, $Z_{iso}B$ is about 5000 ppm[14] and L is 0.5936 nm[35] giving $d\delta_{iso}/dL \cong 2.5 \times 10^4$ ppm nm^{-1}. Similarly, for PbSe and PbTe, $Z_{iso}B$ are about 5400 and 6300 ppm, respectively.[14] With appropriate dimensions (0.6124 nm for PbSe and 0.6454 nm for PbTe[35]), one predicts derivatives $d\delta_{iso}/dL$ between 2.6×10^4 ppm nm^{-1} and 3.0×10^4 ppm nm^{-1}. These estimates of the derivatives from the studies of the pressure dependence are in remarkably close agreement with the derivatives, both in sign and in magnitude, derived from the experimental thermal behavior of $Pb(NO_3)_2$, $PbMoO_4$, and $PbCl_2$ (Table 1) and with the calculated behavior of PbI_6^{4-} (Table 3). This agreement supports the proposition that the thermal behavior of the isotropic shift of [207]Pb in these solid materials reflects mainly the effects of lattice expansion.

Fayon et al.[10] have correlated the lead chemical shift with average lead−oxygen distance in a set of materials containing oxygen atoms showing that compounds with larger average lead−oxygen distances are more shielded. This trend is opposite to that observed by us for changes of Pb−X distance within a single expanding structure. Apparently, the chemical nature of the ligand influences the [207]Pb chemical shift in larger measure than does the Pb−ligand distance alone.

V. Conclusions

The temperature dependencies of the chemical shift tensor of lead $Pb(NO_3)_2$, $PbMoO_4$, and $PbCl_2$ have been documented. By comparison to the known thermal expansion of the unit cell in these materials, we derived the dependence of NMR chemical shift parameters on the characteristic length, $L = V^{1/3}$, of these materials. The results are expressed as derivatives of the various chemical shift parameters with respect to the characteristic length. These are of the order 3×10^4 to 5×10^4 ppm nm^{-1} for the isotropic chemical shift and -1×10^4 to -5×10^4 ppm nm^{-1} for the span of $Pb(NO_3)_2$, $PbMoO_4$, and $PbCl_2$. In the case of $PbCl_2$, the skew was found to be independent of temperature within experimental error.

We have used DFT-ZORA calculations on model clusters to predict dependencies of the isotropic shift and span on structure. The derivatives with respect to interatomic distance are of similar orders of magnitude and sign as the experimental results. An extensive set of calculations on PbI_6^{4-} shows that the isotropic chemical shift depends strongly on the local structure. The dependence of isotropic shift on the interatomic distance is linear, but the span is nonlinear. The span is found to be linear in the angular deviation of the cluster from octahedral symmetry tending toward zero as the lattice expands.

The experimental and theoretical results are also in agreement with recent measurements of the dependence of chemical shift parameters on pressure in similar materials.[14] This confirms that the temperature dependence that has been reported many times for materials like $Pb(NO_3)_2$ is a reflection of changes in the local structure.

These results, taken together, provide a consistent picture of chemical shielding in materials containing heavy nuclei like lead. Changes of structure affect both the paramagnetic and spin−orbit contributions to the shielding. To get semiquantitative agreement of calculation with experiment, one must calculate all contributions to the shielding, and that requires a treatment

of the system as containing relativistic particles.[15,22,23,33] We have found that a cluster model representing the immediate local structure of the lead center semiquantitatively accounts for the observed experimental results. The strong dependence of NMR parameters on local geometry suggests the possibility that measured NMR chemical shift parameters and DFT calculations of them may be used to determine elements of local structure including internuclear distances and bond angles.

Supporting Information Available: Cartesian coordinates of PbX_2 fragments and corresponding calculated chemical shieldings including paramagnetic, diamagnetic, and spin−orbit contributions. This material is available free of charge via the Internet at http://pubs.acs.org.

References and Notes

(1) (a) Nolle, A. *Z. Naturforsch., A* **1977**, *32*, 964. (b) Lutz, O.; Nolle, A. *Z. Phys.* **1980**, *36B*, 323.

(2) Sharma, S.; Weiden, N.; Weiss, A. *Z. Naturforsch., A* **1987**, *42*, 1313.

(3) Nizam, M.; Allavena, M.; Bouteiller, Y.; Suits, B. H.; White, D. *J. Magn. Reson.* **1989**, *82*, 441.

(4) Grutzner, J. B.; Stewart, K. W.; Wasylishen, R. E.; Lumsden, M. D.; Dybowski, C.; Beckmann, P. A. *J. Am. Chem. Soc.* **2001**, *123*, 7094.

(5) Van Bramer, S. E.; Glatfelter, A.; Bai, S.; Dybowski, C.; Neue, G.; Perry, D. L. *Magn. Reson. Chem.* **2006**, *44*, 357.

(6) Neue, G.; Dybowski, C.; Smith, M. L.; Hepp, M. A.; Perry, D. L. *Solid State Nucl. Magn. Reson.* **1996**, *6*, 241.

(7) Neue, G.; Dybowski, C.; Smith, M. L.; Barich, D. H. *Solid State Nucl. Magn. Reson.* **1994**, *3*, 115.

(8) Dybowski, C.; Smith, M. L.; Hepp, M. A.; Gaffney, E. J.; Neue, G.; Perry, D. L. *Appl. Spectrosc.* **1998**, *52*, 426.

(9) Dybowski, C.; Neue, G. *Prog. Nucl. Magn. Reson. Spectrosc.* **2002**, *41*, 153.

(10) Fayon, F.; Farnan, I.; Bessada, C.; Coutures, J.; Massiot, D.; Coutures, J. P. *J. Am. Chem. Soc.* **1997**, *119*, 6837.

(11) Zhao, P.; Prasad, S.; Huang, J.; Fitzgerald, J. J.; Shore, J. S. *J. Phys. Chem. B* **1999**, *103*, 10617.

(12) Bussian, D. A.; Harbison, G. S. *Solid State Commun.* **2000**, *115*, 95.

(13) (a) van Gorkom, L. C. M.; Hook, J. M.; Logan, M. B.; Hanna, J. V.; Wasylishen, R. E. *Magn. Reson. Chem.* **1995**, *33*, 791. (b) Ferguson, D. B.; Haw, J. F. *Anal. Chem.* **1995**, *67*, 3342. (c) Mildner, T.; Ernst, H.; Freude, D. *Solid State Nucl. Magn. Reson.* **1995**, *5*, 269. (d) Beckmann, P. A.; Dybowski, C. *J. Magn. Reson.* **2000**, *146*, 379.

(14) Zwanziger, J. W.; Werner-Zwanziger, U.; Shaw, J. L.; So, C. *Solid State Nucl. Magn. Reson.* **2006**, *29*, 113.

(15) Briand, G. G.; Smith, A. D.; Schatte, G.; Rossini, A. J.; Schurko, R. W. *Inorg. Chem.* **2007**, *46*, 8625.

(16) Mason, J. *Solid State Nucl. Magn. Reson.* **1993**, *2*, 285.

(17) Jameson, C. J. *Sol. State Nucl. Magn. Reson.* **1998**, *11*, 265.

(18) Van Bramer, S. E.; Glatfelter, A.; Bai, S.; Dybowski, C.; Neue, G. *Concepts Magn. Reson.* **2002**, *14*, 365.

(19) (a) Van Geet, A. L. *Anal. Chem.* **1970**, *42*, 679. (b) Van Geet, A. L. *Anal. Chem.* **1968**, *40*, 2227.

(20) The Inorganic Crystal Structure Database (ICSD) is copyrighted by Fachinformationszentrum Karlsruhe and the National Institute of Standards and. Technology. Information on the database is available at http://icsdweb.fiz-karlsruhe.de/. The structure files are listed in Table 2.

(21) Amsterdam Density Functional Program (ADF), 2006.01. See the Supporting Information for the full list of authors.

(22) (a) Schreckenbach, G.; Ziegler, T. *J. Phys. Chem.* **1995**, *99*, 606. (b) Schreckenbach, G.; Ziegler, T. *Int. J. Quantum Chem.* **1996**, *60*, 753. (c) Schreckenbach, G.; Ziegler, T. *Int. J. Quantum Chem.* **1997**, *61*, 899.

(23) (a) Wolff, S. K.; Ziegler, T. *J. Chem. Phys.* **1998**, *109*, 895. (b) Wolff, S. K.; Ziegler, T.; van Lenthe, E.; Baerends, E. J. *J. Chem. Phys.* **1999**, *110*, 7689.

(24) Vosko, S. H.; Wilk, L.; Nusair, M. *Can. J. Phys.* **1980**, *58*, 1200.

(25) Becke, A. D. *Phys. Rev. A* **1988**, *38*, 3098.

(26) Perdew, J. P. *Phys. Rev. B* **1986**, *33*, 8822.

(27) The calculation used $r_{Pb-C} = 2.238$ Å: Oyamada, T.; Iijima, T.; Kimura, M. *Bull. Chem. Soc. Jpn.* **1971**, *44*, 2638.

(28) Harris, R. K.; Becker, E. D.; Cabral de Menezes, S. M.; Goodfellow, R.; Granger, P. *Pure Appl. Chem.* **2001**, *73*, 1795.

(29) Bielecki, A.; Burum, D. P. *J. Magn. Reson. A* **1995**, *116*, 215.

(30) Vegard, L.; Roer, K. I. *Avh. Nor. Vidensk. Akad. Oslo 1: Mat. Naturvidensk. Kl.* **1941**, *14*, 3.

(31) Sillen, L.; Nylander, A. *Ark. Kemi, Mineral. Geol.* **1943**, *17A*, 1.

(32) Straumanis, M.; Sauka, J. *Z. Phys. Chem.* **1943**, *51B*, 219.

(33) Ooms, K J.; Feindel, K. W.; Willans, M. J.; Wasylishen, R. E.; Hanna, J. V.; Pike, K. J.; Smith, M. E. *Solid State Nucl. Magn. Reson.* **2005**, *28*, 125.

(34) Willis, B. T. M.; Pryor, A. W. *Thermal Vibrations in Crystallography*; Cambridge University Press: London, 1975.

(35) Noda, Y.; Masumoto, K.; Ohba, S.; Saito, Y.; Toriumi, K.; Iwata, Y.; Shibuya, I. *Acta Crystallogr., C* **1987**, *43*, 1443.